

# Chapter 1

## Introduction

### 1.1 History of Breadboards

The breadboard has been a staple substrate for electronic construction over the last century. At the dawn of a growing interest in amateur radio, resourceful tinkerers used planks of wood to secure and ruggedize their electrical handiwork. Conductive nodes, such as nails or copper rails, were driven into the non-conductive boards, providing anchors and contact points that were electrically isolated from the rest of the circuit. Components were soldered or wire-wrapped to the nodes, and sometimes secured by non-energized nails or screws. This construction technique provided a lot of artistic freedom in circuit construction, but was time consuming and required relatively heavy hand tools such as a hammer or drill. From a performance perspective, sensitive high-frequency circuits were infeasible due to a lack of a ground plane and long wires between components.

### 1.2 Modern Breadboards

The solderless breadboard is the canonical tool given to students taking introductory courses in the field. Rather than driving nodes into arbitrary locations, component leads are inserted into contact points arranged on a grid that allow rapid semi-rigid construction of circuits with no other tools. The layout of a solderless breadboard is designed to be compatible with a plethora of powerful integrated circuits - enabling complex electronic designs - but is still limited to low-frequency operation due to the parasitic capacitance between adjacent breadboard rails. Modern solderless breadboards have come a long way from their namesake

wooden ancestors, but there is still room for improvement.

The intent of breadboarding is to physically realize a circuit. Often, this involves designing or using a reference schematic to guide construction, but circuit improvisation is not uncommon. A meticulous breadboarder can successfully realize a circuit without error by correctly placing components and jumper wires - taking care not to introduce undesired 'parasitic' components. However, for the uninitiated it is difficult to justify the additional time and care required to plan and build. Inserting components and jumper wires into contact points is straightforward, but poor contacts, broken wires (inside insulation), and mis-inserting leads can plague designers for hours on end and potentially destroy components. Breadboarding is a skill that is learned over time, but small errors can lead to excessive frustration and turn students off to the field. I propose a solution to some of the issues with the solderless breadboard.

A confident linkage between the the electrical and mechanical domains is required to construct a circuit. On larger scales, the mechanical structures (eg. contacts, wires, components) that create electrical circuits are visible in plain sight. It is simple and reliable, then, to determine the circuit representation of a mechanical structure that has no hidden connections. Breadboards often obscure connections due to their construction. The regular nature of a breadboard, a grid of contact points arranged in rails, makes it difficult to keep track of which rail is connected to what circuit node. When combined with the opaque nature of most components and the poor reliability of breadboard contacts, visually verifying complex circuits on a breadboard becomes infeasible. Many of the inherent problems with breadboards stem from this open-loop nature of breadboarding, where visual cues are not enough to determine the electrical circuit from the mechanical structure. A symptom of open-loop construction techniques is a mismatch between the mental model and the physical realization of the system at hand. I seek to close this loop by designing and implementing a circuit-sensing breadboard.

### 1.3 Proposed Solution

A circuit-sensing breadboard is able to reverse-engineer circuits built on it by applying test voltages and currents and measuring the results. As a proof-of-concept, the proposed circuit-sensing breadboard completed for this thesis is able to reverse engineer circuits composed of

resistors, inductors, and capacitors built on a small section of the breadboard and display the circuits as a schematic in the browser.

The circuit-sensing breadboard is composed of a hardware system that interfaces various pieces of test equipment with eight rails on a breadboard. The system is composed of a pcb-mounted breadboard, a voltage source, current meter, and voltage meter multiplexing board, a microcontroller development board, firmware to control ADC sampling, AC voltage source testing, and streaming data to a computer for analysis and display. The hardware is controlled by a circuit sensing algorithm, which determines the equivalent circuit elements between any two nodes on the breadboard. A software simulation of the hardware system verifies operation of the network sensing algorithm and enables testing for networks larger than eight nodes. Once the circuit sensing algorithm reconstructs the entire circuit it generates a schematic diagram of the circuit, closing the loop on breadboard construction.

## **1.4 Implementation to Date**

Made the software test bench, an 8-rail hardware test bench, and got the network sensing algorithm working for resistors with resistance between 100 and 5K  $\Omega$ .



# Chapter 2

## Theory

The design of a Network Sensing Algorithm requires an understanding of the networks to be analyzed. In this thesis, the networks of interest are composed of three circuit elements: resistors, capacitors, and inductors. The constitutive relations for these electrical circuit elements relate the voltage across an element to the current passing through it as a function of time. In this application, it is useful to reinterpret the constitutive relations as a function of frequency by taking the Fourier Transform.

### 2.1 RLC Elements

The constitutive equations that define current and voltage relations in the elements of interest are as follows:

Resistive element behavior is characterized by a linear relationship between current and voltage. That is,  $v = iR$

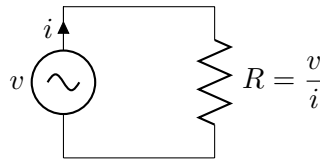


Figure 2-1: Constitutive Relations for Resistance

Inductive element behavior is characterized by a linear relationship between the time derivative of current and voltage. That is,  $v = L \frac{di}{dt}$

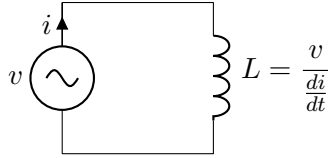


Figure 2-2: Constitutive Relations for Inductance

Capacitive element behavior is characterized by a linear relationship between the time derivative of voltage and current. That is,  $i = C \frac{dv}{dt}$

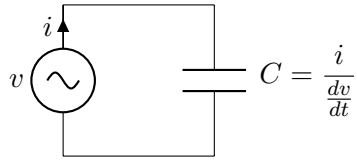


Figure 2-3: Constitutive Relations for Capacitance

Given current and voltage measurements taken from an element, it is possible to determine the type of element by matching the measurement with the correct constitutive relation.

## 2.2 Frequency Domain Perspective

Laplace transform of:

$$v = iR, v = L \frac{di}{dt}, \text{ and } i = C \frac{dv}{dt}$$

$$V = IR, V = LsI, I = CsV$$

Impedance:

$$Z_R = R, Z_L = Ls, Z_C = \frac{1}{Cs}$$

## 2.3 Network Analysis

KVL KCL

## 2.4 Network Sensing Algorithm

Given access to the set of nodes in an electrical network, the objective of a network sensing algorithm is to determine the set of branches and the elements that compose them. In order to illustrate how a network sensing algorithm operates, it is necessary to begin with a simple example and then build in complexity.

The ability to ground arbitrary nodes of a network greatly simplifies the process of analyzing and reverse-engineering a network. The network-sensing algorithm relies on the ability to shrink the effective network by conglomerating nodes into the ground node.

### 2.4.1 Two Node Network

Take the example of a network with two nodes below:

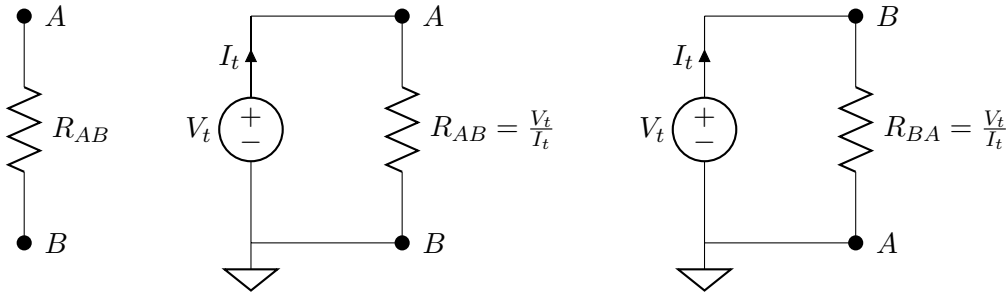


Figure 2-4: Finding  $R_{AB}$  in a two node network

In the case of a resistive network with two nodes, there is only one possible branch in the network and thus one possible element to characterize. From elementary circuit theory, the resistance between two nodes equal to the voltage across the nodes divided by the current through the nodes when power is applied. Here, the resistance  $R_{AB}$  is found by placing a test voltage  $V_t$  across the nodes and measuring the resulting current,  $I_t$ , then taking the ratio  $\frac{V_t}{I_t}$ . This measurement is called the driving point impedance <sup>1</sup>. If there are no circuit elements between the two nodes, the driving point impedance test will find zero current in the test voltage source, resulting in an infinite resistance between two nodes. An infinite resistance between two nodes in a circuit indicates that there are no elements in that branch of the network. Thus, the network can subsequently be simplified by removing that branch

<sup>1</sup>To measure a driving point impedance, a test voltage is applied between the node of interest and ground, and the resulting current in the voltage source is measured. The driving point impedance is then computed by dividing the test voltage by the resulting current.

from the network.

### 2.4.2 Three Node Network

A resistive network with two nodes is simple, but provides an introduction to the methodology used in analyzing larger networks. In the case of a resistive network with three nodes, it is insufficient to utilize driving point impedance measurements alone, because each node has more than one path to any other node.

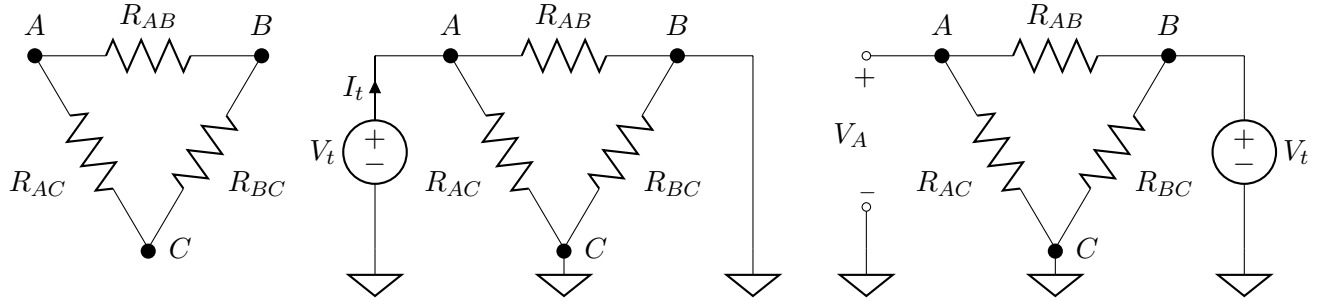


Figure 2-5: Finding  $R_{AB}$  in a three node network

Consider a resistive network with three nodes: A, B, and C. In order to determine the resistance in branch AB, the driving point impedance at node A is measured with nodes B and C grounded. This provides the resistance of the parallel combination of the branches with an endpoint at node A:<sup>2</sup>

$$R_{A||} = R_{AB} || R_{AC}$$

Next, a test voltage source is applied to node B, node C is grounded, and the voltage at node A,  $V_A$ , is observed.

$$V_A = V_t \frac{R_{AC}}{R_{AB} + R_{AC}} = V_t \frac{R_{AB} || R_{AC}}{R_{AB}} = V_t \frac{R_{A||}}{R_{AB}}$$

The branch resistance of interest,  $R_{AB}$  is calculated using the known quantities  $V_t$ ,  $V_{A||}$ , and  $V_A$ .

$$R_{AB} = V_t \frac{R_{A||}}{V_A}$$

This procedure is repeated for the remaining branches to determine the entire network.

---

<sup>2</sup> $R_1 || R_2 = \frac{R_1 R_2}{R_1 + R_2}$



### 2.4.3 N Node Network

A resistive network with any number of nodes can be reduced to a resistive network with three nodes by grounding the nodes that are not of interest. The resulting network does not modify the branch of interest, but connects the remaining branches attached to the nodes of interest in parallel. This collapses the network into a three node network or three branch equivalent circuit. Consider a resistive network with five nodes: A-E. To determine

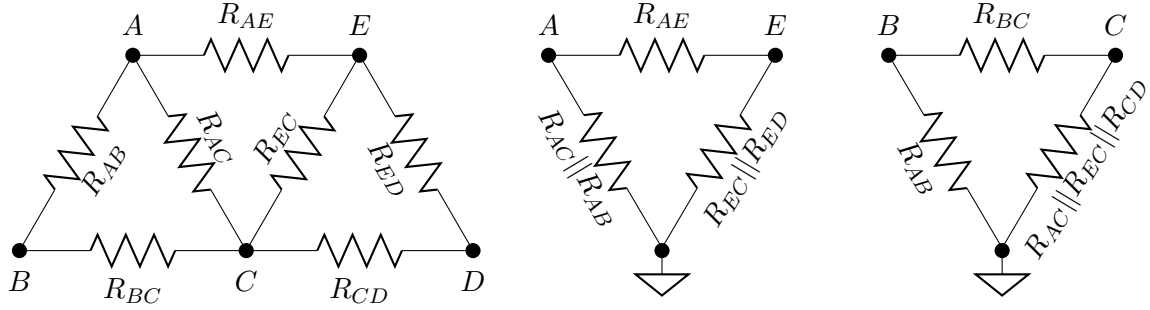


Figure 2-6: Collapsing five node network, collapsed to find  $R_{AE}$  and  $R_{BC}$

the resistance between nodes A and E, the network is reduced to a three-node network by connecting all nodes except nodes A and E to ground. The three resistances of the branches that remain are  $R_{AE}$ ,  $R_{AB} || R_{AC}$ , and  $R_{EC} || R_{ED}$ . The reduced network is then solved using the three node network method, and this procedure is repeated for all branches in the network.

The above thought experiment satisfies the problem at hand intuitively, but it can also be shown mathematically.

To find  $R_{AB}$  of an n-node complete network, first the driving point impedance at node A,  $R_{A||}$ , is measured with all other nodes grounded.

$$\begin{aligned}
 R_{A||} &= R_{AB} || R_{AC} || R_{AD} || \dots = \frac{1}{\frac{1}{R_{AB}} + \frac{1}{R_{AC}} + \frac{1}{R_{AD}} + \dots} \\
 &= \frac{1}{\frac{1}{R_{AB}} + \left( \frac{1}{\frac{1}{R_{AC}} + \frac{1}{R_{AD}} + \dots} \right)} \\
 &= R_{AB} || (R_{AC} || R_{AD} || \dots)
 \end{aligned}$$

To find  $V_A$  from node B, the voltage at node A is measured when a test source is placed at

node B with all other nodes grounded.

$$V_A = V_t \frac{(R_{AC} || R_{AD} || \dots)}{R_{AB} + (R_{AC} || R_{AD} || \dots)}$$

Dividing  $R_{A||}$  by  $V_A$  and multiplying by  $V_t$ :

$$V_t \frac{R_{A||}}{V_A} = V_t \frac{\frac{R_{AB}(R_{AC} || R_{AD} || \dots)}{R_{AB} + (R_{AC} || R_{AD} || \dots)}}{V_t \frac{(R_{AC} || R_{AD} || \dots)}{R_{AB} + (R_{AC} || R_{AD} || \dots)}} = R_{AB}$$

Finding a resistive element in an n-node network requires two measurements. The number of branches in a complete graph with n nodes is equal to  $\frac{n(n-1)}{2}$ . The total number of measurements required to reverse-engineer an n-node circuit is  $n(n-1)$ .

#### 2.4.4 Element Identification

Networks composed of elements with complex impedance can be analyzed with the same algorithm. By replacing the test DC voltage sources with AC voltage sources, the imaginary reactance of capacitors and inductors can be measured in addition to the real resistance of resistors.

#### From Resistance to Impedance

Chapter 2 described the use of the Laplace Transform to characterize the behavior of circuit elements in the frequency domain. Here, frequency-domain complex impedance is useful for identifying circuit elements based on the change in branch impedance over inputs of various frequencies.

MAKE NOTE ABOUT USING THE AMPLITUDE OF THE MEASURED SIGNALS

#### Parallel RLC Branches

To determine if there are multiple element types [in parallel] between two nodes, the impedance is measured over a range of frequencies, and the resulting changes in impedance are measured.

The impedance of a parallel RLC 'tank' circuit can be characterized and analyzed over all frequencies.

$$Z_R = R \quad Z_L = j\omega L \quad Z_C = \frac{1}{j\omega C}$$

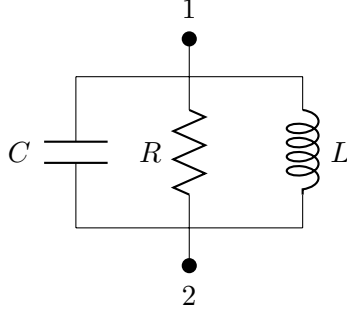
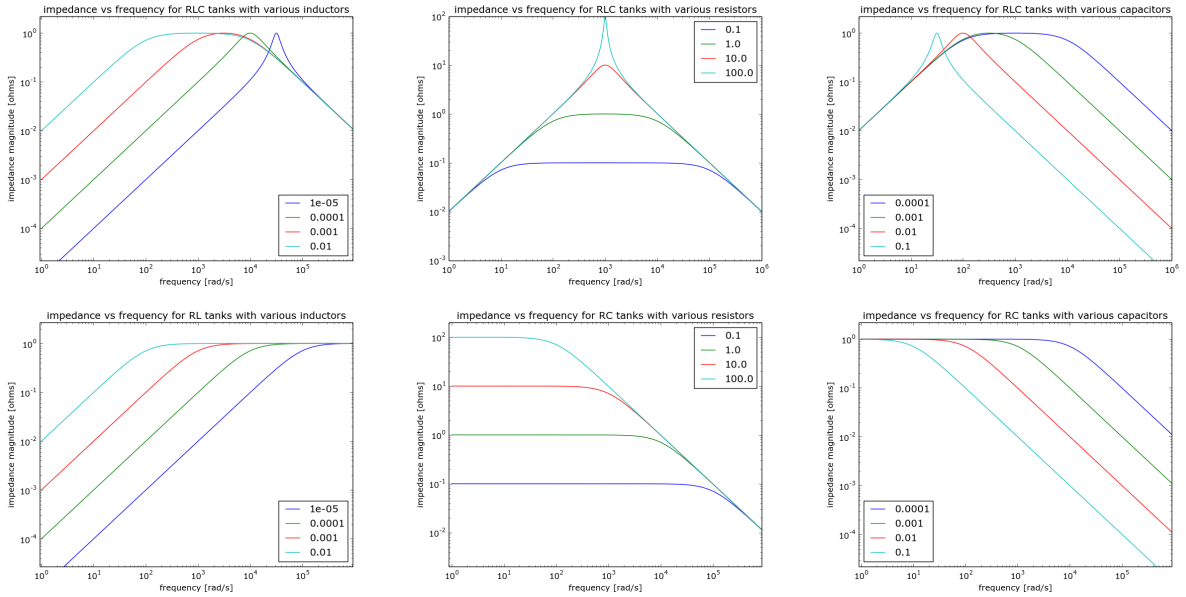


Figure 2-7: Example RLC Tank Circuit

$$Z_{RLC} = Z_C || Z_R || Z_L = \frac{1}{j\omega C + \frac{1}{R} + \frac{1}{j\omega L}} = \frac{j\omega RL}{-\omega^2 RLC + j\omega L + R}$$

$Z_{RLC}$  has a zero at  $\frac{1}{RL}$  and two poles at  $\frac{-L \pm \sqrt{L^2 + 4R^2 LC}}{-2RLC}$



The plots above illustrate various RLC tank circuits where one component value changes over several orders of magnitude. In the top-center and bottom-center plots, a decrease in resistance drops the maximum impedance over all frequencies. In the top-left and bottom-left plots, a decrease in inductance drops the asymptotic impedance at low frequencies. In the top-right and bottom-right plots, a decrease in capacitance drops the asymptotic impedance at high frequencies. As illustrated above, there are three regimes on the impedance vs frequency plot that divide the operation of an RLC tank into three elements:

When the slope of  $|Z|$  vs.  $f$  is +1, the tank behaves like an inductor with inductance

$$L = |Z|/(j\omega)$$

When the slope of  $|Z|$  vs.  $f$  is -1, the tank behaves like a capacitor with capacitance

$$C = j\omega|Z|$$

When the slope of  $|Z|$  vs.  $f$  is 0, the tank behaves like a resistor with resistance

$$R = |Z|$$

### Finite Difference Stencil

To reliably determine the regions of effective resistance, inductance, and capacitance, the slope of the  $\log(|Z_{nm}|)$  vs.  $\log(\omega)$  is computed via the midpoint method. The midpoint finite difference stencil takes the two points on either side of the point of interest and computes the slope between them.

$$Z'[n] = \frac{1}{2}(Z[n+1] - Z[n-1])$$

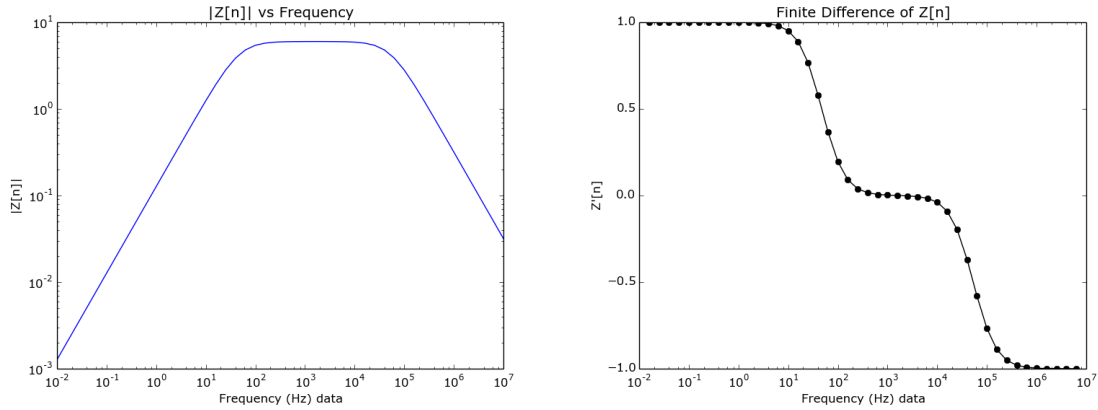


Figure 2-8: Finite difference of an RLC tank where  $R=6\Omega$ ,  $L=20\text{mH}$ , and  $C=500\text{nF}$

In figure ?? the distinct regions of inductance, resistance, and capacitance are clearly visible and easily found by setting thresholds for the finite difference. The thresholds on

the region of inductance are between 1.1 and 0.9, the thresholds on the region of resistance are between 0.1 and -0.1, and the thresholds on the region of capacitance are between -0.9 and -1.1.

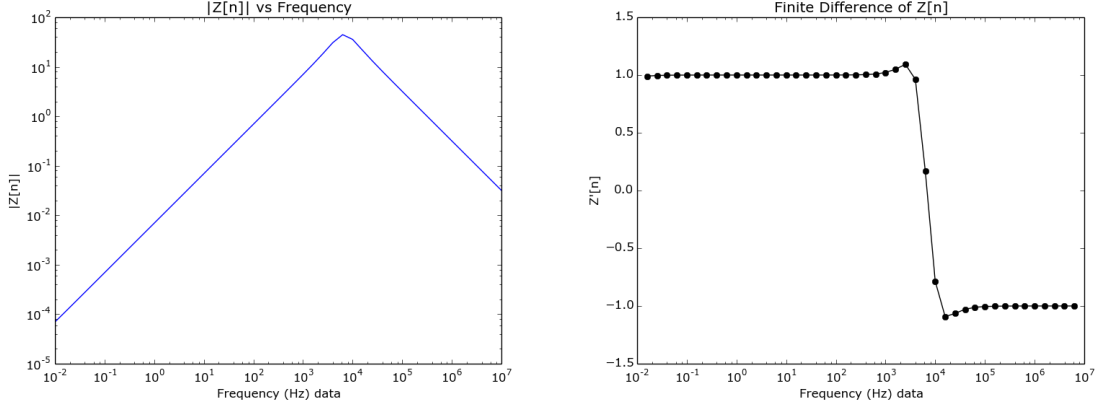


Figure 2-9: Finite difference of an RLC tank where  $R=44\Omega$ ,  $L=1.1\text{mH}$ , and  $C=500\text{nF}$

In figure ??, the resistance is not represented in the finite difference of  $Z[n]$ . The parallel resistance of an underdamped RLC tank is the maximum recorded impedance across all frequencies. In a simulation, using the maximum recorded impedance is a valid solution because measurement accuracy has a large (64-bit floating point) dynamic range, producing results that are accurate of ideal systems. In practice, spurious noise and lack of dynamic range over measurement data can cause poor results. Occasionally these poor results include large spikes of inaccurate impedance readings, which can range from  $10^{12}$  to  $10^{-12}$ . In this case, a practical approach would be to use the finite difference stencil where possible and when an LC network is discovered, sample at the resonant frequency to find  $R$ . In the case of figure ??, the sampling frequency would be 17KHz.

$$f_0 = \frac{1}{\sqrt{2\pi LC}} \approx 17000\text{Hz}$$

### Component Value Calculation

Once the regions of the impedance plot are thresholded, the sampling frequency domains corresponding to those regions are assigned to an element type  $[\omega_r[n]$  for  $R$ ,  $\omega_l[n]$  for  $L$ ,  $\omega_c[n]$  for  $C$ ]. The for each sampling frequency, the component values are computed and then

averaged to counter noisy data.

$$R[\omega_r] = Z[\omega_r] \quad L[\omega_l] = \frac{Z[\omega_l]}{\omega_l} \quad C[\omega_c] = \frac{1}{\omega_c Z[\omega_c]}$$

$$R = \frac{1}{rnum} \sum_{\omega_r} Z[\omega_r] \quad L = \frac{1}{lnum} \sum_{\omega_l} \frac{Z[\omega_l]}{\omega_l} \quad C = \frac{1}{cnum} \sum_{\omega_c} \frac{1}{\omega_c Z[\omega_c]}$$

Where  $rnum$ ,  $lnum$ , and  $cnum$  are the number of sample frequencies in the R, L, and C regions, respectively.

### 2.4.5 Reconstructing the Network

With a record of all of the elements and their connections in the network, the network can be reconstructed and a schematic of the original circuit is drawn.

## Chapter 3

# Simulation

A simulation was built to test the Network Sensing Algorithm before embarking on hardware design. In addition to the rapid prototyping cycle, the implementation of NSA and automated schematic drawing were directly used later on. The simulation generates random networks of resistors, inductors, and capacitors, and proceeds to analyze and reconstruct the network using NSA.

### 3.1 NgSpice and Netlists

The open source software package NgSpice was used to simulate the networks and test circuits applied to the network. NGspice operates on text files called netlists, where each component in the network is specified on a single line. An example netlist is shown below.

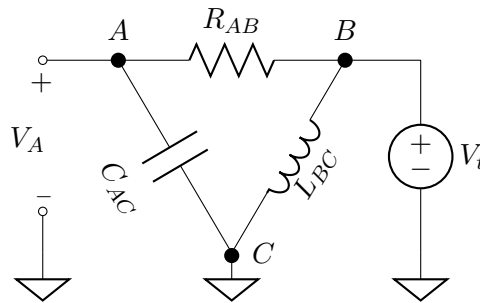


Figure 3-1: Five node network

```
fiveNodeNetlist
```

```
Vt 0 B 1
```

```

Rab A B 10k
Cac A C 1e-6
Lbc B C 1e-3
Vcg 0 C 0
.control
op
print(v(A))
.endc
.end

```

The first letter of each element line designates the element to simulate:

**V** **start stop value** → Voltage Source between **start** and **stop** nodes, **value** Volts [V]  
**R** **start stop value** → Resistor between **start** and **stop** nodes, **value** Ohms [ $\Omega$ ]  
**L** **start stop value** → Inductor between **start** and **stop** nodes, **value** Henries [H]  
**C** **start stop value** → Capacitor between **start** and **stop** nodes, **value** Farads [F]

Node 0 is always designated as ground, and all simulations require a ground node.

The control commands are as follows:

**op** → Operating Point Simulation **print()** → Print the relevant data passed as an argument  
**v(N)** → The voltage at node N **i(E)** → The current through element E

## 3.2 Methods

The NSA simulator was written in python and uses the methods below.

### 3.2.1 Generate Random Netlist

```
writeRandomNet(netlist,num,elements):
```

Generates **num**-node random graph with no self-linking nodes (symmetric matrix with zeros on the diagonal) for each [**elements**] type (R,L,C). Subsequently assigns random values between two realistic limits for each element and writes the network to netlist **netlist**.  
 1-1k ohms, 10nF-10uF, 100uH-100mH.

When writing the capacitive and inductive elements, care must be taken to prevent a DC operating point simulation from failing. The infinite resistance across a capacitor and



zero resistance across an inductor are responsible for DC operating point simulation failure, and can be fixed by including a small resistor in series with inductors and a large resistor in parallel with capacitors.

<pre>L0 1 2 1mH  →  L0 1 t10 1mH                 R10 t10 2 1e-5</pre>	<div style="border-left: 1px solid black; height: 100%; margin: 0 10px;"></div>	<pre>C0 1 2 1e-6F  →  C0 1 2 1e-6F                 Rc0 1 2 1e8</pre>
---	---	--

### 3.2.2 Inserting Voltage Sources, Grounds and Probes

`insertProbe2(target,nodes,groundNodes,probes,source='DC'):`

Inserts a 1V voltage source from ground to each node in `[nodes]`, grounds each node in `[groundNodes]`, and adds a voltage print statement for each node in `[probes]`. By default, the voltage sources are written as DC sources, but if 'AC' is passed into the last argument the sources are written as AC sources and the AC control statement is added.

```
AC dec 5 10m 10meg
```

Which runs a small-signal AC simulation and returns the amplitudes of the resulting voltage and current waveforms, five sample point per decade from 10mHz to 10MHz.

### 3.2.3 Run Simulation

`def runSim(target,results,source='DC'):`

Makes a system call to NgSpice in batch mode with netlist `target` and outputs the result to text file `results`. The last argument indicates how to parse the resulting data, as NgSpice returns DC data in the following format:

```
No. of Data Rows : 1
i(v) = -1.18295e-01
v(5) = 2.532846e-07}
```

and AC data is returned in this format:

```
No. of Data Rows : 6

                                mynetlist
                                AC Analysis  Sun Aug 30 18:35:07  2015
-----
Index   frequency             i(v)
-----
0        1.000000e+00         -1.72598e+00,      3.978810e+02
1        1.000000e+01         -1.58689e-01,      3.978827e+01
```

2	1.000000e+02	-1.43015e-01,	3.974287e+00
3	1.000000e+03	-1.42859e-01,	3.520201e-01
4	1.000000e+04	-1.42857e-01,	-4.18884e-01
5	1.000000e+05	-1.42857e-01,	-4.58275e+00

mynetlist

AC Analysis Sun Aug 30 18:35:07 2015

```
-----
Index   frequency      v(3)
-----
0        1.000000e+00    1.000000e+00,    0.000000e+00
1        1.000000e+01    1.000000e+00,    0.000000e+00
2        1.000000e+02    1.000000e+00,    0.000000e+00
3        1.000000e+03    1.000000e+00,    0.000000e+00
4        1.000000e+04    1.000000e+00,    0.000000e+00
5        1.000000e+05    1.000000e+00,    0.000000e+00
```

### 3.2.4 Print Matrix

`def printMatrix(m):` Prints matrix `m` in nice command-line output.

## 3.3 Executing NSA

### 3.3.1 Calculate $Z_{n||}(f)$

$Z_{n||}(f)$  is found by grounding all nodes except for node `n` and adding a voltage source to that node, then taking the ratio of the amplitudes of the resulting current into the node of interest and the voltage source.

### 3.3.2 Calculate $V_n(f)$

$V_n(f)$  is found by grounding all nodes except for nodes `n` and `m`, adding a voltage source to node `m`, and measuring the amplitude of the voltage at node `n`.

### 3.3.3 Calculate $Z_{nm}(f)$

$Z_{nm}(f)$  is calculated by the ratio of  $Z_{n||}(f)$  to  $V_n(f)$  scaled by  $V_t$ . In the case of this simulation,  $V_t$  is one.

#### **3.3.4 Finite Difference**

#### **3.3.5 Element Identification**

#### **3.3.6 Network Reconstruction**

### **3.4 Output to JSON**

Blah Blah

### **3.5 D3?**

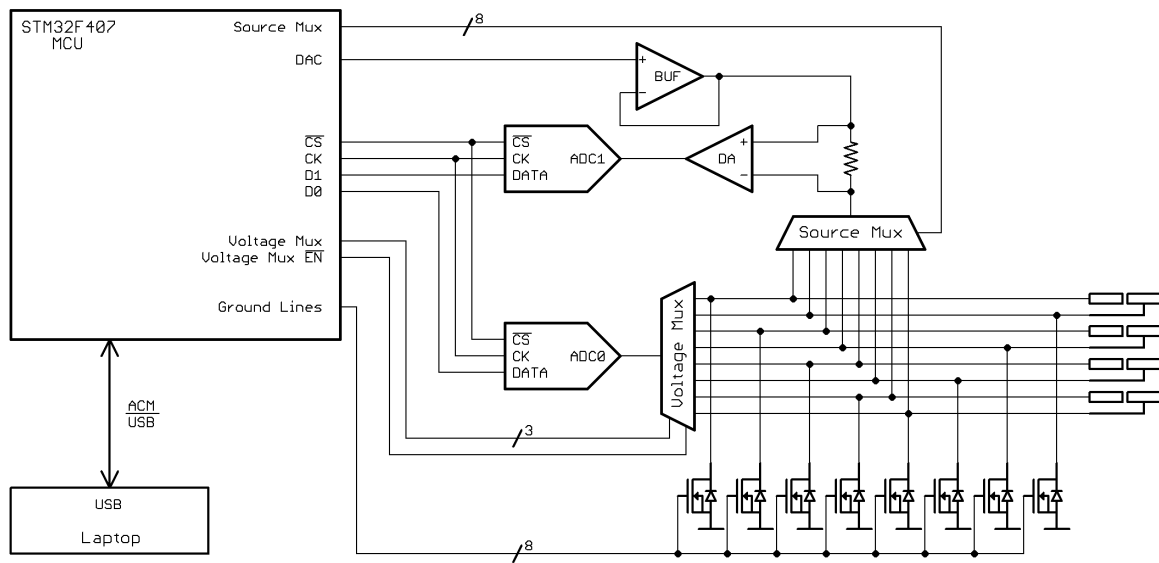
???? maybe



# Chapter 4

## Hardware

Block diagram / Schematic



### 4.1 Low Cost

Keeping the cost of production low makes butterboard accessible to the largest population of people. Using multiplexed ADCs where possible keeps the cost down by reducing the quantity of high price-tag components, like ADCs.

## 4.2 Node Voltage Reading

An ADCS7476 12-bit A/D converter is used to measure the voltages at each node. The ADCS7476 can sample up to 1MSPS with  $\pm 1$  LSB of total unadjusted error from  $-40^{\circ}\text{C}$  to  $85^{\circ}\text{C}$  and  $< \pm 0.2$  LSB of error at  $25^{\circ}\text{C}$ . No bits are wasted in the ADCS7476 A/D converter. Additionally, the input circuitry to the ADC is a  $100\Omega$  resistor in series with a 26pF capacitor. This places a pole at 61MHz, causing a .03% error at 100KHz and .3% error at 1MHz. The additional performance is well worth the additional cost of \$1.56375 in quantities of 1Ku.

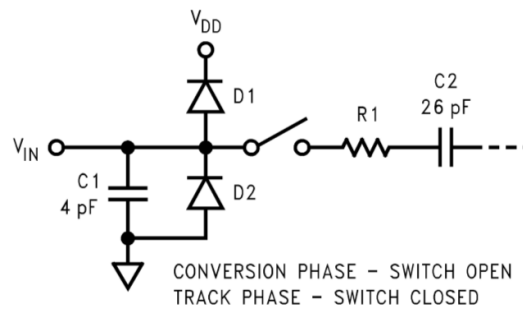


Figure 4-1: ADCS7476 Equivalent Input Circuit

The ADC is connected to the common pin of a CD4051 1:8 analog multiplexer. The multiplexer is connected to eight breadboard rails, which allows the ADC to measure the voltage on any of the eight rails, one rail at a time.

The CD4051 has about  $200\Omega$  of series resistance and 30pF of output capacitance when its supply voltage is 12V, which places an additional pole at 26MHz, again well above the Nyquist frequency.

So far, the voltage-reading signal chain has two poles - one at 61MHz and one at 26MHz.

### 4.2.1 Onboard A/D converters

Although the STM32F407 has three onboard 12-bit A/D converters, their specifications are lacking. Each is able to sample at 2MSPS, and it's possible to interleave them to attain a sampling rate of 6MSPS or higher if you're willing to throw away bits. The total unadjusted error (offset error, gain error, differential linearity error, and integral linearity error) is between  $\pm 2$  LSB and  $\pm 5$  LSB. With a minimum of  $\pm 2$  LSB's of error, the lowest significant two bits in the 12-bit A/D are virtually useless. Another specification to consider

is the input circuitry to the ADC. The input circuitry to the ADC while it's in tracking mode looks like a  $6K\Omega$  resistor charging a  $4pF$  capacitor. This puts a pole at  $6.6MHz$ , causing .3% error in measurement at  $100KHz$ , 3% error in measurement at  $1MHz$ , and 7% at  $3MHz$ . When sampling at the maximum sample rate of  $6MSPS$ , the ADC's input network begins to introduce significant error. Granted, it's likely that there will be an alternative bandwidth bottleneck, this is still a metric of concern. [DM00037051.pdf, pages 133-134]

### 4.3 Signal Generator

The STM32F407 has an onboard D/A converter that is good enough to use as a signal generator. The onboard DAC is configured to output a cosine wavetable with a DC offset, as described in the next chapter.

### 4.4 Test Voltage Current Sensing

The DAC output is buffered by half of an MCP6L92  $10MHz$  op-amp. The onboard DAC can be configured with an optional onboard buffer, but the buffer limits the DAC output range from  $0.2V$  to  $V_{dd}-0.2V$ . Without the onboard buffer, the DAC output is  $15k\Omega$ . When configured as a voltage buffer, the MCP6L92 has an input impedance larger than  $1G\Omega$ , resulting in no signal attenuation.

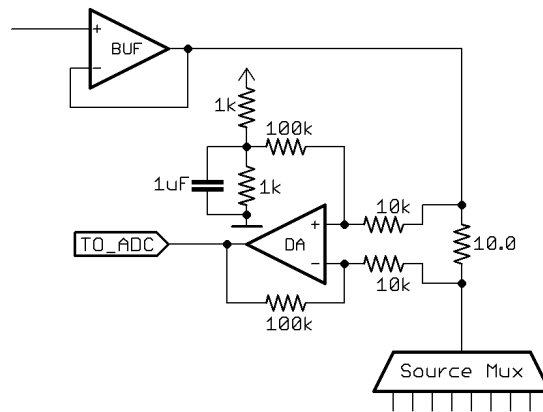


Figure 4-2: Difference Amplifier Schematic

The buffer sources current through a  $10.0\Omega$ , 1% sense resistor, which can be switched onto any of the breadboard rails through an array of eight high-side switches. The voltage

across the sense resistor is measured by the other half of the MCP6L92 op-amp configured as a simple difference amplifier. Using two  $10\text{k}\Omega$  resistors and two  $100\text{k}\Omega$  resistors, the difference amplifier is configured with a gain of 10.

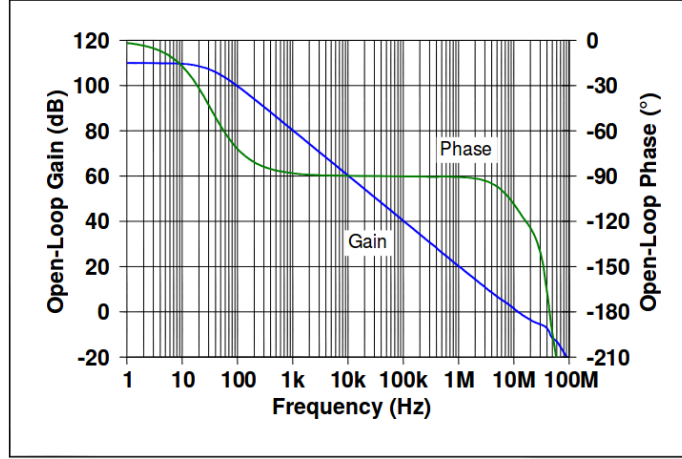


Figure 4-3: MCP6L92 Open Loop Bode Plot

According to the MCP6L92 datasheet, the difference amplifier should have a -3dB bandwidth of 1MHz and plenty of phase margin driving the  $100\Omega$ - 26pF input impedance to the current sense ADC.

## 4.5 High-side Switches

The high-side switches were selected for high-voltage operation, so that any rail of the breadboard could swing between 0 and 30V and there wouldn't be a problem. The selected switches were Vishay DG468 normally open analog switches. They have  $9\Omega$  resistance and 76pF of capacitance in the on-state, 1nA of leakage current and 30pF of capacitance in the off-state. The high and low side switches are the main limits of bandwidth due to their high amounts of input capacitance in both on and off states.

## 4.6 Low-side Switches

The low-side switches have a low logic-level threshold voltage, low drain-source on-resistance, can handle up to 30V, and are low-cost. The IRLML2803 N-FETs have an  $R_{DS_{ON}}$  of about  $1\Omega$  with a  $V_{GS}$  of 3.3V. With 10V  $V_{GS}$ ,  $R_{DS_{ON}}$  drops to  $250\text{m}\Omega$ . The downside of these



FETs is the high  $C_{DS}$  that comes from a wide transistor.  $C_{DC}$  is on the order of 60pF for each transistor. When combined with the additional capacitances mentioned above, each breadboard rail has a total of 140pF to ground. This has a significant impact on the maximum usable frequency for even moderate impedances on the breadboard. For example, consider a 10k $\Omega$ -10k $\Omega$ resistor divider. At 100kHz, the 140 pF capacitance on each rail has 11k $\Omega$ of impedance.

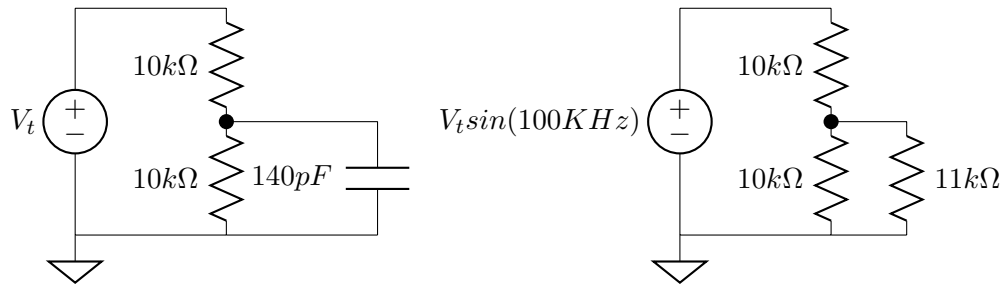


Figure 4-4: Resistor Divider Parasitic Capacitance

## 4.7 PCB Mounted Breadboard

## 4.8 Hardware Prototypes



## Chapter 5

# Firmware

The firmware is structured in three sections - USB data reception and transmission, DAC operation, and ADC operation.

Libopencm3, licensed under the GNU LGPL v3, is used extensively in this firmware.

Block Diagram

### 5.1 ADC

The ADCS7476 is a successive approximation ADC with an SPI interface. In operation, a master device initiates a conversion by pulling  $\overline{CS}$  low, then clocks in data using the  $CK$  line and reading  $SDATA$ .

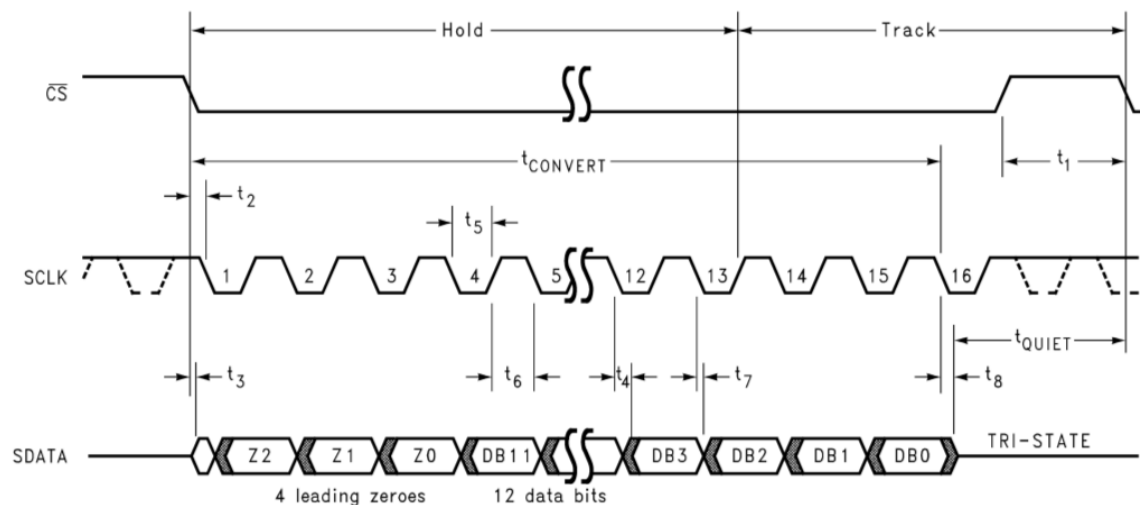


Figure 5-1: ADCS7476 Serial Interface Timing Diagram

The ADC firmware configures two 32-bit timers and the DMA to record data from up to sixteen external ADCs. The two timers are responsible for driving the Chip Select and Clock lines on all of the ADCs. The timing of the Chip Select line determines the sampling frequency and the Clock line is driven at the ADCS7476's maximum clock frequency of 20MHz. On the rising edge of each clock cycle, the DMA is triggered to sample the data lines of each ADC. A trigger causes the DMA to store each of the 16 pin states on **PORT E** as a 16-bit integer in the buffer **datas**.



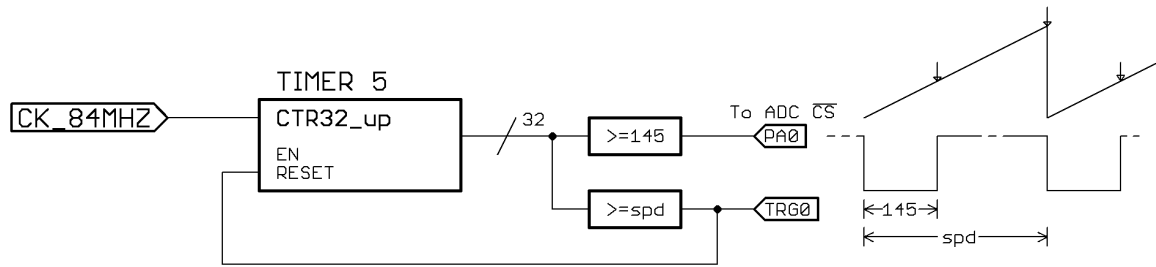


Figure 5-3: ADC Chip Select Timer

Timer 1 drives the ADC Clock lines and behaves as a  $1\mu S$  on -  $1\mu S$  off 16-shot timer. It's also configured as a 32-bit up-counting timer clocked at 84MHz, but it's only enabled by the TRG0 signal from Timer 5. Like Timer 5, it uses output compare unit 1 to control an output pin, in this case PA8. Unlike Timer 5, it's set to run in one-shot mode with a repetition counter that is preloaded with a value of 15. The output compare unit is set to run in PWM2 mode with fixed compare and update registers. When Timer 1 counts to 5, the compare unit fires and PA8 goes high. When the count reaches 10, the timer is updated, PA8 goes low, and the repetition counter decrements. The timer continues to run, toggling PA8 and decrementing the repetition counter, until the repetition counter reaches a value of 0. Once the repetition counter reaches 0, the next Timer 1 update disables the timer.

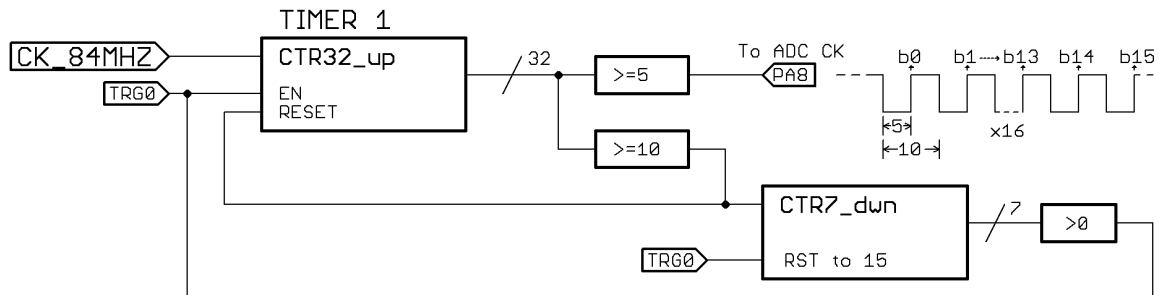


Figure 5-4: ADC Clock Timer

### 5.1.2 ADC DMA

A DMA controller is used to store serial ADC data from up to 16 ADCs in parallel. On each clock cycle, DMA2 takes the 16-bit integer value represented by the state of the 16 pins on PORT E and stores it in memory. As shown in Figure ??, the ADC data pin is updated on a falling clock signal. To record the state of the data pin, DMA2 is triggered to start a data

transfer on every compare event from Timer 1, which corresponds with the rising edge of the clock signal.

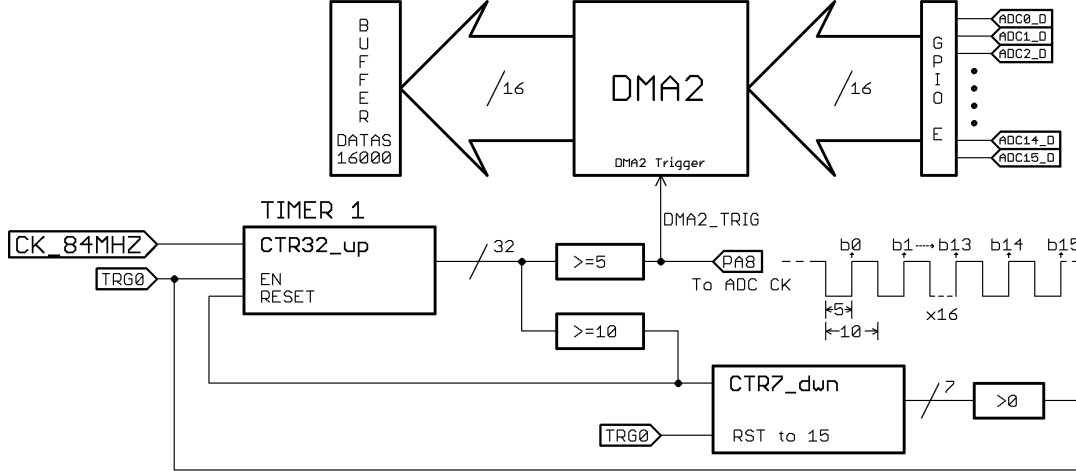


Figure 5-5: ADC Clock Timer Triggers DMA2

When Timer 5 is enabled, DMA2's 'number of data' [to transfer] register is set to 16000 and the ADCs continuously sample at the sample period defined by `spd`. In each cycle of Timer 5, Timer 1 toggles the clock line 16 times, triggering DMA2 on each rising edge. With each DMA trigger, DMA2's number of data register decrements. When the register reaches 0, an interrupt fires that disables Timer 5 and begins the data reconstruction process.

### 5.1.3 Data Reconstruction

Since the serial data stream from each ADC is stored sequentially, the actual A/D readings need to be reconstructed after they are recorded. In Figure ??, the binary data stored in `datas` is examined. Each 16-bit integer in `datas` contains one bit of data from each of the 16 pins on PORT E, which connect to the data pins on the external A/D converters. Here, each letter represents the data from a particular external ADC.

To reconstruct the data collected from  $ADC_a[0]$ , a routine iterates through `datas[0:15]`, summing appropriately bit-shifted  $b_0$ 's.

$$ADC_a[0] = (a_{15} \ll 15) + (a_{14} \ll 14) + (a_{13} \ll 13) + \dots + (a_2 \ll 2) + (a_1 \ll 1) + a_0$$

To reconstruct all of the waveform recorded, the routine iterates through `datas[0:16000]`,

Bit Index	$b_{15}$	$b_{14}$	$b_{13}$	$b_{12}$	...	$b_3$	$b_2$	$b_1$	$b_0$
<code>datas[0]</code>	$p_{15}$	$o_{15}$	$n_{15}$	$m_{15}$	...	$d_{15}$	$c_{15}$	$b_{15}$	$a_{15}$
<code>datas[1]</code>	$p_{14}$	$o_{14}$	$n_{14}$	$m_{14}$	...	$d_{14}$	$c_{14}$	$b_{14}$	$a_{14}$
<code>datas[2]</code>	$p_{13}$	$o_{13}$	$n_{13}$	$m_{13}$	...	$d_{13}$	$c_{13}$	$b_{13}$	$a_{13}$
<code>datas[3]</code>	$p_{12}$	$o_{12}$	$n_{12}$	$m_{12}$	...	$d_{12}$	$c_{12}$	$b_{12}$	$a_{12}$
$\vdots$	$\vdots$	$\vdots$	$\vdots$	$\vdots$	...	$\vdots$	$\vdots$	$\vdots$	$\vdots$
<code>datas[13]</code>	$p_2$	$o_2$	$n_2$	$m_2$	...	$d_2$	$c_2$	$b_2$	$a_2$
<code>datas[14]</code>	$p_1$	$o_1$	$n_1$	$m_1$	...	$d_1$	$c_1$	$b_1$	$a_1$
<code>datas[15]</code>	$p_0$	$o_0$	$n_0$	$m_0$	...	$d_0$	$c_0$	$b_0$	$a_0$
<code>datas[16]</code>	$p_{15}$	$o_{15}$	$n_{15}$	$m_{15}$	...	$d_{15}$	$c_{15}$	$b_{15}$	$a_{15}$

Figure 5-6: `datas[0:16]`

reconstructing 1000 samples from each ADC.

After reconstruction, the data is sent to a host program over USB for further processing.

## 5.2 DAC

The STM32F407's onboard DAC is used as a signal source for impedance testing. The DAC is configured to update on a timer, and is fed new waveform values from a wavetable by DMA1.

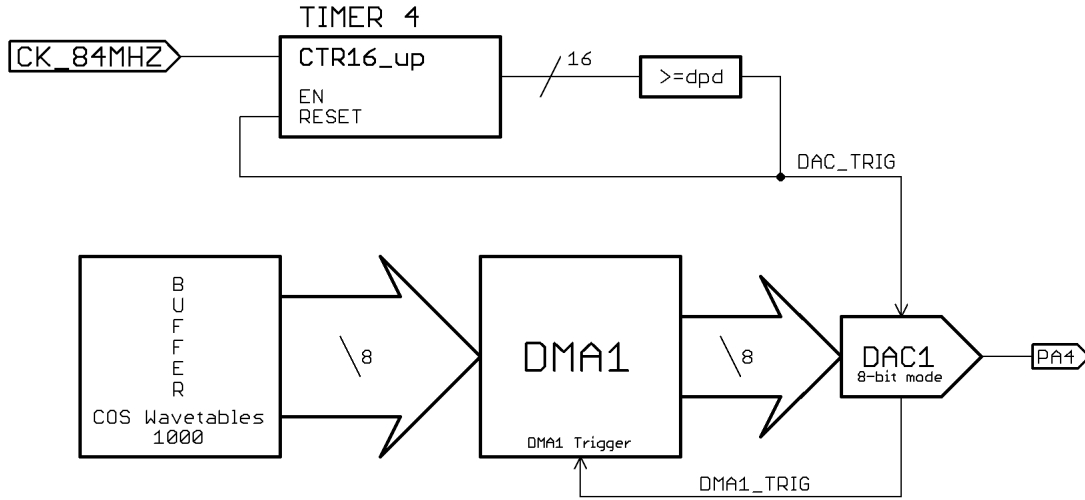


Figure 5-7: DAC Timer Triggers DMA1

Timer 4 is configured as a 16-bit up-counting timer with period `dpd`, set by command



over USB. On update, Timer 4 is a master to DAC1, and triggers the DAC to output a new value. The DAC, in turn, triggers a data transfer from DMA1, which transfers the next value in the cosine wavetable to DAC1.

### **5.2.1 DAC Wavetables**

There are three DAC wavetables, each 1000 bytes long. The first wavetable has four cycles of cosine, the second has 10, and the last has 40. The different-sized wavetables are necessary to maintain high-fidelity output signals at low frequency while still permitting high-frequency output.

## **5.3 USB**

### **5.3.1 USBACM**

### **5.3.2 Command List**